13.6 THE ROLE OF EVAPORATIVE PROCESSES IN GRAVITY WAVE GENESIS

Brian F. Jewett*, Mohan K. Ramamurthy and Robert M. Rauber

Department of Atmospheric Sciences
University of Illinois at Urbana-Champaign, Urbana, IL

1. INTRODUCTION

The genesis of large-amplitude mesoscale gravity waves (MGWs) has been a topic of active research for many years. In the United States, such waves are most common east of the Rocky mountains (Koppel et al. 2000), and are normally accompanied by cloud bands and precipitation (Koch and O'Handley 1997, Koppel et al. 2000). The close relationship between precipitation and gravity waves has been documented in both warm- and cool-season events, but the origins of this relationship are often unclear. Koch and Golus (1988) and Powers and Reed (1993) concluded that gravity waves and convective motions are interdependent and thus difficult to distinguish from one another.

Because data limitations have hampered the understanding of wave genesis mechanisms, specialized data sets, field experiments and modeling studies have been used in attaining much of our understanding of these waves. An observational study was carried out by Rauber et al. (2000, Part I) and Yang et al. (2000, Part II) for a gravity wave occurring during the STORM Fronts Experiment Systems Test (STORM-FEST). Utilizing profiler, surface mesonet, 3-hourly rawinsonde and dual-Doppler measurements as the wave moved through the STORM-FEST network, they concluded that evaporation to the rear of a rainband accompanying the wave was important to wave structure. In this study, modeling of this event was used to investigate wave genesis and evolution prior to the mature structure revealed by Parts I and II. While many theories exist to explain wave genesis, our emphasis is on the relationship between the precipitation band and gravity wave, and the role of evaporation.

2. METHODOLOGY

Numerical simulations of the 14 February 1992 gravity wave were carried out with the nonhydrostatic Penn. State/NCAR MM5 mesoscale model (Grell et al. 1995). The model initialization was obtained through an analysis of upper air and surface data from 0000 UTC 14 February 1992, 15.5 hours prior to observed gravity wave genesis. This early time was chosen to allow model spinup and to ensure that the MGW formation was not a model artifact or a consequence of initialization. National Centers for Environmental Prediction (NCEP, then NMC) global tropospheric analyses were used as first-guess fields. After interpolation to the model vertical (sigma) coordinate, removal of integrated divergence was performed to reduce noise in the initial condition fields.

Three grids were employed, with 54, 18 and 6-km horizontal resolution. The 6-km innermost grid spacing is considered adequate to resolve the gravity wave structure given the observed wavelength of 35 to 60 km from Doppler radar and Portable Automated Mesonet (PAM) observations presented in Part I. The outer two grids were initialized at 0000 UTC, while the innermost 6-km nest was initiated at 0600 UTC and moved eastward (at 1200 and 1800 UTC) to follow the lee cyclone and developing gravity wave. High vertical resolution (62 sigma layers) was utilized to limit spurious waves in the model, particularly in the region of observed MGW genesis.

As in Powers (1997), explicit grid-scale microphysics followed the simple ice parameterization of Dudhia (1989). The Grell cumulus scheme, which includes the effect of moist downdrafts, was used for cumulus parameterization on all grids. The Blackadar boundary layer was employed. In addition to saving traditional model fields every 15 minutes, surface wind, pressure, temperature, moisture, low-level cloud and rainwater mixing ratio, and four levels of vertical velocity were stored at *each* 90s model time step.

3. WAVE GENESIS AND MATURE STRUCTURE

The 14 February 1992 gravity wave event accompanied a lee cyclone, which moved from Colorado into Kansas during the day. At 1200 UTC (Fig. 1A), the surface low-pressure center was located in eastern Colorado in the simulation, slightly north of the observed position. A warm front extended east from the cyclone center and a dryline was present to the south. Behind the dryline, strong westerly winds and dry air extended back to the Rocky Mountains of New Mexico and southern Colorado. The cyclone was associated with the left exit region of a jetstreak over west Texas at 1200 UTC (not shown). A well-developed

* *Corresponding author address*: Brian F. Jewett, Department of Atmospheric Sciences, 216 Atmos Sci. Bldg., 105 S. Gregory St., Urbana, IL 61801. Email: jewett@atmos.uiuc.edu

comma-cloud structure was evident in the model relative humidity (RH) fields (Fig. 1B) and infrared satellite imagery. A large-scale dry slot (Fig. 1B, dark shading) was evident above the shallow moist air mass (Fig. 1B, hatched region) north of the surface warm front. The gravity wave and associated rainband formed in the model and observations within this larger dry slot.

Koch and Siedlarz (1999, hereafter KS99) identified three gravity waves across Kansas by 1810 UTC on this day. The most significant of these waves formed in the southwestern part of the state near 1530 UTC, accompanied by a cloud band. The modeled gravity wave appeared in the MM5 surface pressure and wind fields near 1800 UTC in association with a precipitation band aloft. Wave genesis took place north of the surface warm front in the left exit region of the jet, as in the Uccellini and Koch (1987) climatology. The gravity wave structure on the innermost 6-km grid at 2000 UTC is shown in Fig. 2.

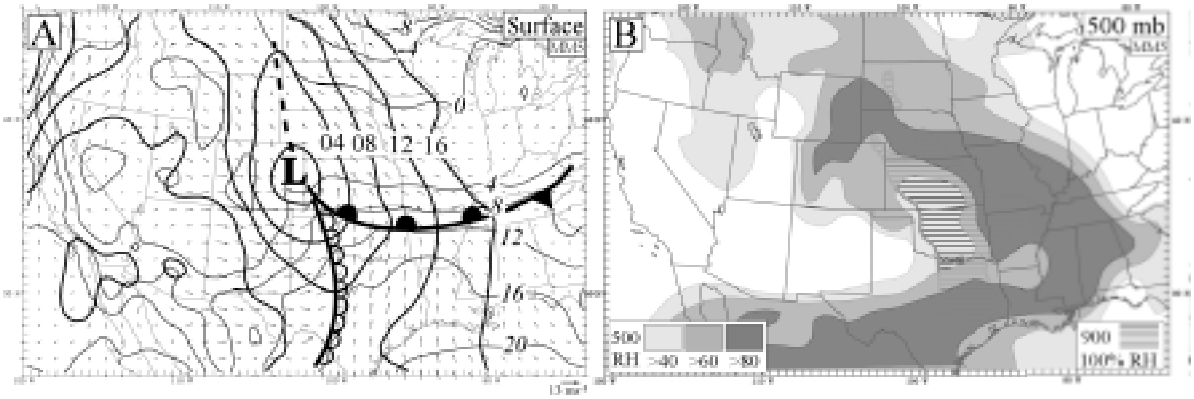

Fig. 1: 12-hour, 54-km MM5 forecast valid 1200 UTC. A: MSL pressure (-1000 mb, dark), surface temperature (ºC), wind vectors (every 2nd) and fronts. B: 500 mb relative humidity (shaded, %) and 900 mb 100% RH area (hatched).

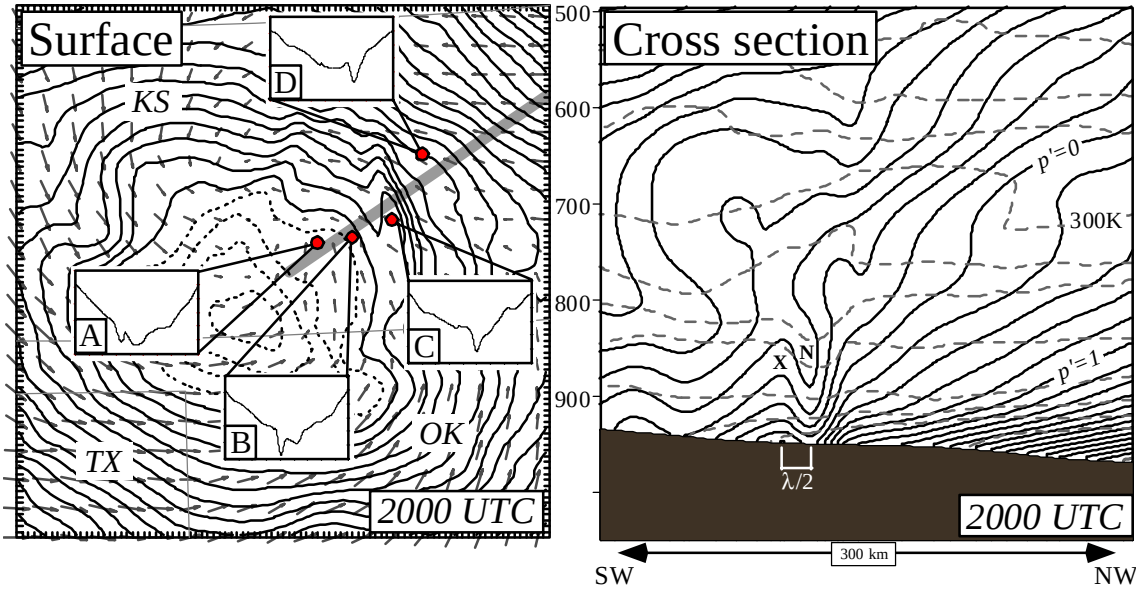

Fig. 2. Left: 2000 UTC surface perturbation pressure (every 0.25 mb, dashed negative) and wind vectors (every 5th). Detrended pressure time series for points A, B, C and D (inset) cover 1500-0000 UTC; the full pressure scale is 5 mb. Right: Cross section (axis on left) of perturbation pressure (solid, every 0.2 mb) and potential temperature (dashed, every 2.5 K). X denotes the pressure ridge, N the trough and λ/2 the half-wavelength.

At 2000 UTC, the wave of depression appeared as an inverted trough of lower surface pressure northeast of the lee cyclone center. The points A, B, C, and D were chosen near the wave axis at 1815, 1900, 2000 and 2100 UTC. MM5 6-km surface data, at 90s resolution, was used to construct the time series profiles at each location. The time series of perturbation pressure were detrended and plotted, revealing the wave of depression in the model fields.

A northeast-southwest cross section through the wave is also shown in Fig. 2. The "X" identifies the local perturbation pressure maximum, and "N" the minimum. The pressure perturbations associated with the wave are most prominent in the lowest 100 mb. The half-wavelength ($\lambda/2$ in the figure) is approximately 16 km, yielding a simulated wavelength of 33 km. This is in good agreement with the 35 km wavelength measured at Topeka, as reported in Part I.

The pressure fall in Fig. 2 was beneath a region of depressed isentropes, indicating warming below 800 mb. Elevated isentropes aloft identifies cooling near 750 mb above the same region. This pattern of potential temperature perturbations and pressure falls maintained considerable temporal continuity (not shown) as the wave propagated northeastward.

While the modeled wave amplitude (1-2 mb) is smaller than observed, the surface manifestation of the wave is clearly evident in the highly correlated wind and pressure perturbations found in the 6-km model data (Fig. 3). When the u'p' correlation was computed for three overlapping three-hour time periods over all 6-km grid points, the wave propagation was clear as the area of high (exceeding 0.9) correlation progressed northeastward through 2300 UTC. When computed for a 3-hour period centered on the detrended pressure minimum at each grid point, the result was the large region of high correlation seen in Fig 3B.

The wave isochrones also appear in Fig. 3. Surface evidence of genesis first occurred near 1800 UTC in the simulation, as a wave of depression developed. The modeled wave propagated east-northeast at 12.5 m s^{-1} between 1900 and 2100, slower than the observed speed of nearly 20 m s^{-1}. This discrepancy is consistent with the slower movement of the modeled surface cyclone relative to the observations.

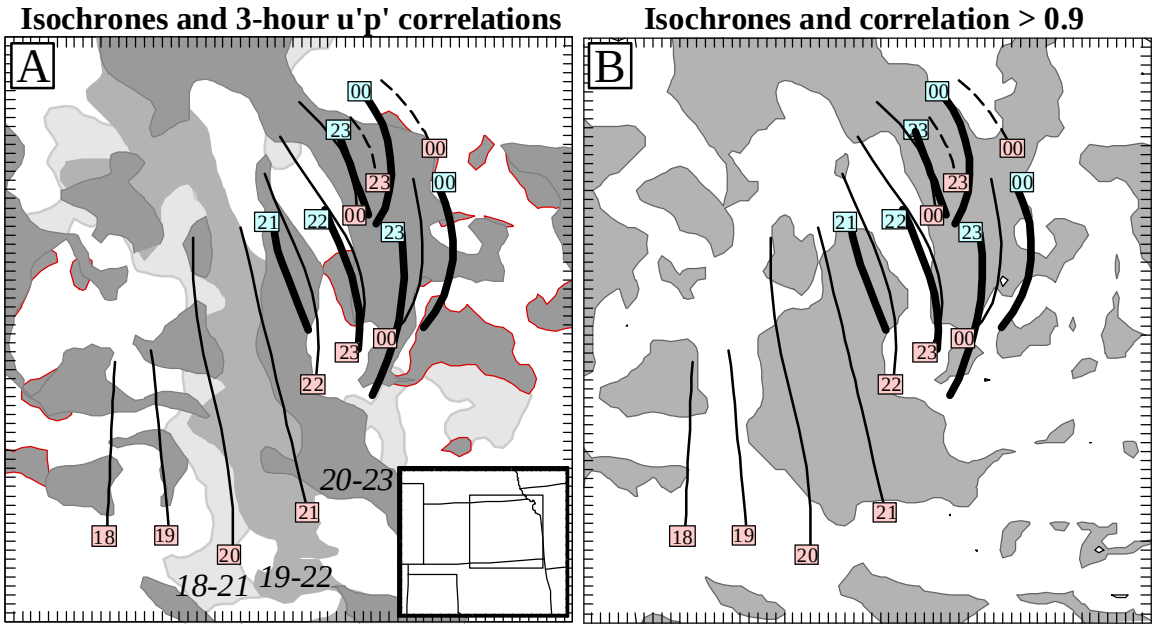

Fig. 3. Left: isochrones and regions with correlation exceeding 0.9. Isochrones are drawn with thin (thick) lines denoting wave of depression (elevation) at 1-hour intervals, with the hour (UTC) shown. Correlation regions are for 1800-2100, 1900-2200 and 2000-2300 UTC. Map at lower right shows analysis region. Right: isochrones and region of correlation exceeding 0.9 for the time window centered about the detrended surface pressure minimum at each MM5 6-km grid point.

The gravity wave in the model simulation was closely coupled to a precipitation band. At 2100 UTC (Fig. 4B), the isochrone (P^-) marking the wave of depression was located behind a rainband, similar to observed behavior in STORM-FEST (KS99). The perturbation pressure field lagged the low-level vertical velocity field (Fig. 4B) by ¼-wavelength as expected. Subsidence was noted on the periphery of the precipitation region (Fig. 4A) between 700 and 850 mb. This downdraft was strongest above the isentrope depression in Fig. 4A, and was due to evaporation.

Near the trailing edge of the precipitation band, evaporation results in cooling aloft, subsidence, and (for total evaporation) adiabatic warming at lower levels. When the evaporative downdraft impinges on the warm frontal inversion, the inversion depth is reduced and hydrostatic surface pressure falls occur, leading to the development of a wave of depression (Part II; see also Stumpf et al. 1991 and Bauck 1992). As the wave intensifies, highly correlated surface wind and pressure perturbations form (Fig. 3). Thus, the model results directly point to evaporative processes being responsible for wave genesis, as hypothesized in Part II. Although difficult to compare directly with observations, the model evolution is consistent with STORM-FEST data. A cloud band appeared in infrared satellite imagery prior to the surface indication of the wave, which preceded the development of heavy precipitation (KS99). The model results suggest that as the weak rainband first developed, evaporation above the frontal inversion initiated the surface pressure falls and wave genesis.

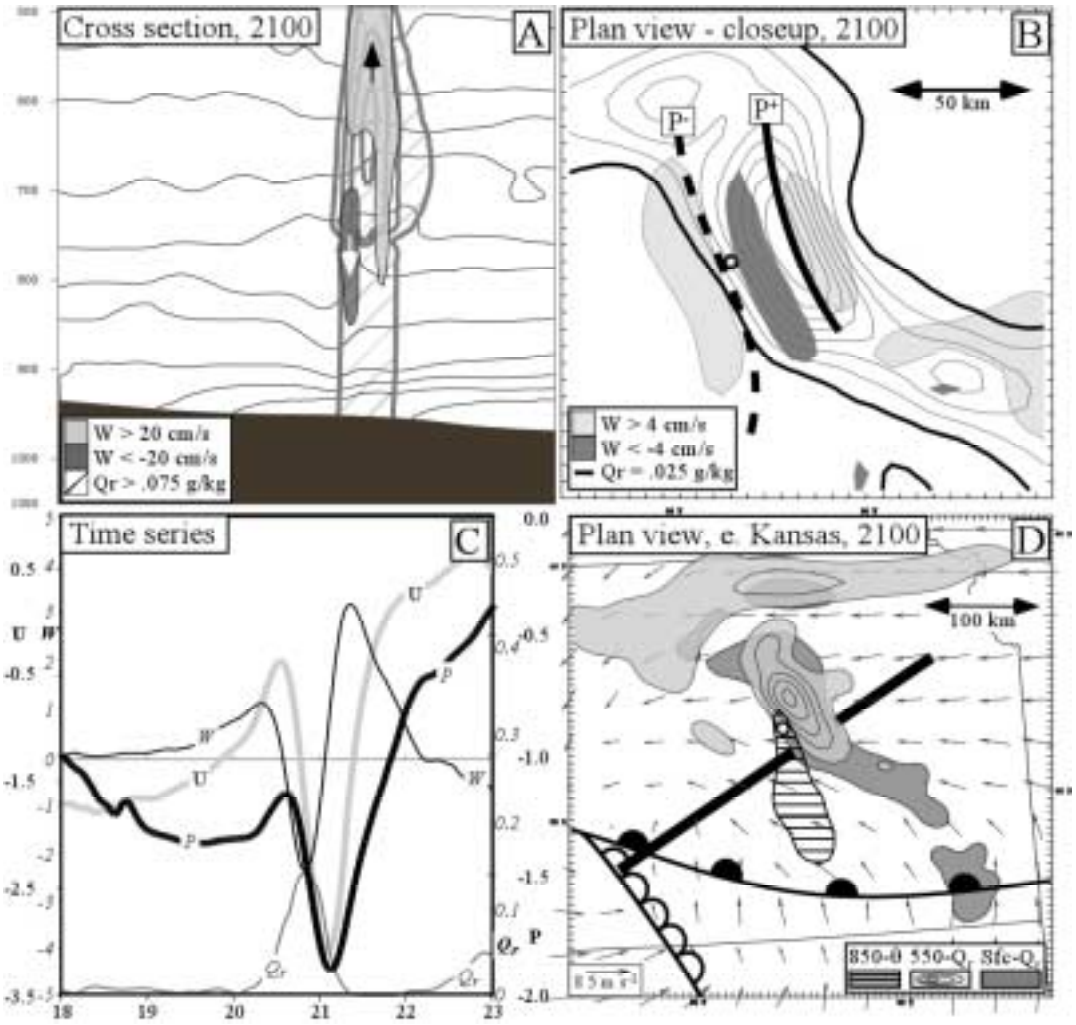

Fig. 4. A: Cross section (axis in 4D) of θ (every 2.5K, thin), rainwater (Q_r, contoured and hatched) and vertical velocity (W, shaded). B: Closeup of surface rainwater (contoured every 0.025 g kg^{-1}), 900 mb vertical velocity (shaded) and isochrones of pressure fall (P^-) and rise (P^+). C: Surface time series (at bold circle in B,D) of wind (U), pressure (P), vertical velocity (W, cm s^{-1}), and rainwater (Q_r). D: surface fronts, rainwater over .05 g kg^{-1}, wind vectors (every 5th), 550 mb rainwater (light shading and contours), and 850 θ exceeding 293.5 K (hatched).

Further simulations were carried out to isolate the role of evaporative processes. We impulsively omitted evaporation *after 1200 UTC*, allowing time to establish most of the cyclone evolution. As a result, evidence of the wave vanished including 850 mb subsidence warming and surface pressure falls. For the case where evaporative processes were restored after 1630 UTC, wave genesis again occurred as in the experiment with full physics.

4. SURGE EVOLUTION AND WAVE GENESIS

Our results show that wave genesis was tied directly to the formation of a weak rainband. The model fields further indicate that the rainband formed ahead of a low- to mid-tropospheric surge of dry air within the larger-scale dry slot. At the surface, the strong westerly winds behind the dryline (Fig. 1A) originated as mountain downslope flow. Trajectory analyses indicate that air at 2 km MSL behind the rainband at 1800 originated at 0600 UTC over central New Mexico. This air descended abruptly in the lee of the Rocky Mountains before advancing through the TX panhandle into southern KS. This dry air likely aided in evaporation of the elevated precipitation from the rainband.

The 650-RH, wind and rainwater field evolution appears in Fig. 5. Model cross sections (not shown) and plan views indicate that the rainband formed between 1400 and 1500 UTC ahead of the leading edge of the dry surge (indicated with shading in the figure). By 1800, a wave of depression had formed at the surface. The gravity wave trough remained tied to the rainband through the remainder of the simulation. The rainband and wave decoupled from the dry surge after 2000 UTC in the model, earlier than in STORM-FEST.

5. DISCUSSION AND SUMMARY

This study has found that wave genesis was in response to evaporative processes acting on precipitation from a weak rainband. The resulting subsidence above the warm frontal inversion resulted in hydrostatic pressure falls and formation of a wave of depression. In effect, a wake low (Johnson and Hamilton 1988) was present, due primarily to depression of the inversion rather than adiabatic warming (the latter partly offset by evaporative cooling). The similarity between gravity waves and wake lows has been noted earlier (Bosart and Seimon 1988, Branick et al. 1988, KS99). We believe we have strongly established the role of evaporative processes and precipitation in wave genesis for this case.

6. ACKNOWLEDGEMENTS

This work was supported by the National Science Foundation under grants ATM-9708170 and ATM-0004274. Discussions with Dr. Steven Koch of NOAA/FSL are gratefully acknowledged.

7. REFERENCES

Bauck 1992, *Wea. Forecasting* **7**, 389-397.
Bosart and Seimon 1988, *Mon. Wea. Rev.* **116**, 1857-1886.
Branick et al. 1988, *Mon. Wea. Rev.* **116**, 1335-1370.
Dudhia 1989, *J. Atmos. Sci.* **46**, 3077-3107.
Grell et al. 1995, NCAR Technical Note TN-398+STR.
Johnson and Hamilton 1988, *Mon. Wea. Rev.* **116**, 1444-1472.
Koch and Golus 1988, *Mon. Wea. Rev.* **116**, 2527-2544.
___ and O'Handley 1997, *Wea. Forecasting* **12**, 253-281.
___ and Siedlarz 1999, *Mon. Wea. Rev.* **127**, 2854-2879.
Koppel et al. 2000, *Mon. Wea. Rev.* **128,** 51-68.
Powers and Reed 1993, *Mon. Wea. Rev.* **121**, 2285-2308.
Powers 1997, *Mon. Wea. Rev.* **125**, 1838-1869.
Rauber et al. 2000, *Mon. Wea. Rev*. **129**, 198–217.
Stumpf et al. 1991, *Mon. Wea. Rev*. **119**, 134-158.
Uccellini and Koch 1987, *Mon. Wea. Rev.* **115**, 721-729.
Yang et al. 2000, *Mon. Wea. Rev.* **129**, 218–236.

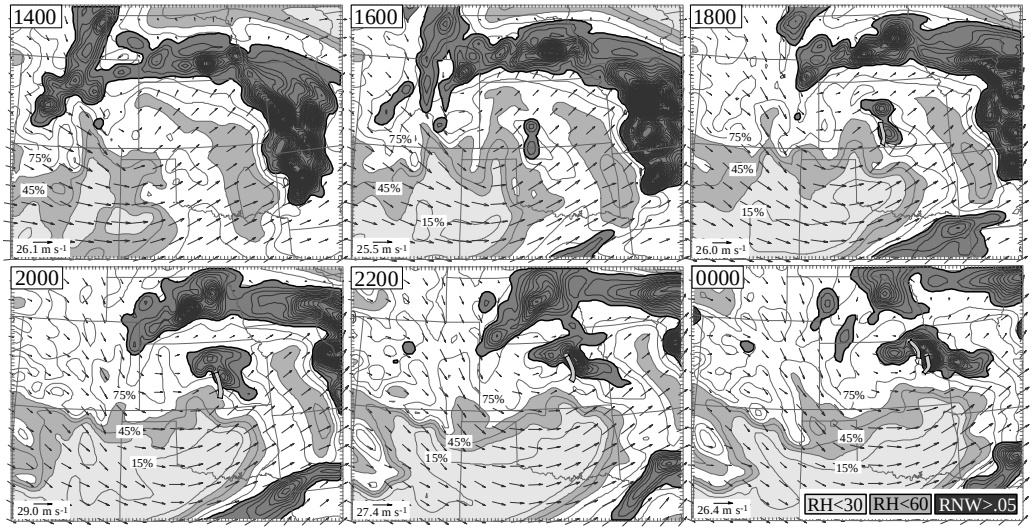

Fig. 5: 650 mb RH (every 15% and shaded below 30, 60%), winds (every 5th, with peak wind at lower left) and rainwater (contoured within dark shading every .05 g kg^{-1}) on the 18-km grid. Isochrones of pressure fall (from 6-km MSL pressure fields) are shown with light line segments at 1800, 2000, 2200 and 0000 UTC.